11-15-2019

Mitigation of Anisotropic Fatigue in Nickel Alloy 718 Manufactured via Selective Laser Melting

Volodymyr P. Sabelkin

Gregory R. Cobb

Travis Shelton

Megan N. Hartsfield

David J. Newell

See next page for additional authors

Recommended Citation

Sabelkin, V. P., Cobb, G. R., Shelton, T. E., Hartsfield, M. N., Newell, D. J., O'Hara, R. P., & Kemnitz, R. A. (2019). Mitigation of anisotropic fatigue in nickel alloy 718 manufactured via selective laser melting. Materials and Design, 182, 108095. https://doi.org//10.1016/j.matdes.2019.108095

Materials and Design 182 (2019) 108095

Contents lists available at ScienceDirect

Materials and Design

journal homepage: www.elsevier.com/locate/matdes

Mitigation of anisotropic fatigue in nickel alloy 718 manufactured via selective laser melting

Volodymyr P. Sabelkin, Gregory R. Cobb*, Travis E. Shelton, Megan N. Hartsfield, David J. Newell, Ryan P. O'Hara, Ryan A. Kemnitz

Air Force Institute of Technology, Department of Aeronautics and Astronautics, 2950 Hobson Way, Wright-Patterson AFB, OH 45433-7765, USA

HIGHLIGHTS

- Fatigue behavior of 3D printed nickel alloy 718 specimens with varying print orientations and heat treatments was studied.
- A modified heat treatment was introduced to induce grain growth and recrystallization.
- The modified heat treated specimens' fatigue behavior was the most isotropic.
- A threshold where the roughness overtakes the print orientation as the force behind fatigue-based failure was discovered.

GRAPHICAL ABSTRACT

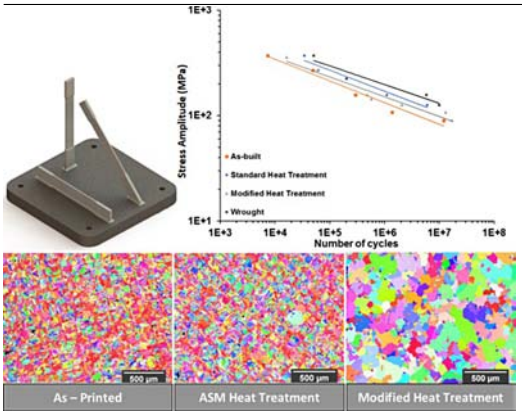

ARTICLE INFO

Article history:
Received 8 July 2019
Received in revised form 30 July 2019
Accepted 1 August 2019
Available online 5 August 2019

Keywords:
Inconel 718
Selective laser melting
Electron backscatter diffraction (EBSD)
Annealing
Fractography
Anisotropy

ABSTRACT

The tension-tension fatigue behavior of heat treated selective laser melted (SLM) nickel alloy 718 (IN718) tensile specimens was tested and compared to as-built specimens. In addition to the industry standard IN718 heat treatment, a modified heat treatment was developed and tested in order to mitigate the anisotropic mechanical properties inherent to SLM materials. Electron backscatter diffraction verified that the modified heat treatment significantly affected the microstructure in all build planes. Three different print orientations were studied to determine their effect on the fatigue behavior. Both heat treatments improved the fatigue life of the specimens, although neither surpassed the fatigue life of wrought specimens. The modified heat treatment reduced the effect of the print orientation on the fatigue life. Surface roughness estimates made by laser scanning microscopy revealed a threshold between roughness controlled fatigue life behavior and print orientation fatigue life dependence. Fracture surface analysis indicated that the print orientation was the greatest factor that influences crack initiation and propagation.

1. Introduction

Selective laser melting (SLM) is a viable alternative to metal forging and casting due to its ability to produce parts with fine details as well as create prototypes that can be implemented into working equipment [1]. SLM research has been performed on metals such as titanium alloy Ti-6Al-4V, stainless steel, and nickel alloy 718 (IN718) [2]. IN718 is an attractive material for SLM components due to its weldability and corrosion resistance. However, the material properties of components made by SLM must be fully understood to ensure they can be safely implemented into existing equipment. The layer-by-layer melting process of SLM causes anisotropy in the

* Corresponding author.
E-mail address: gcobb@afit.edu (G.R. Cobb).

https://doi.org/10.1016/j.matdes.2019.108095

Table 1
Chemical composition of the IN718 used in the wrought and SLM specimens as reported by the manufacturer. Note that there were also trace ($< 0.1\%$) amounts of Mn, Si, S, P, B, Cu, Ca, C, Mg, O, and N.

Element	Ni	Cr	Fe	Nb+Ta	Mo	Ti	Al	Co
% by Weight	54.05	18.08	17.69	5.32	2.93	0.97	0.45	0.2

microstructure of as-printed parts. The grains grown in the build direction are long and columnar, while grains transverse to the build direction are generally equiaxed [3]. As a result, the material properties of SLM parts are dependent on their build orientation, and parts with identical geometries will have unpredictable behavior if the print direction is unknown.

As with traditionally wrought materials, the microstructure of additively manufactured metals can be manipulated by heat treatment. The heat treatment standard AMS 5662 is commonly applied to IN718 components [4], but previous research has shown that it does not induce grain growth or eliminate the columnar grains from printed materials [5–7]. Recent research by Raghavan has shown that annealing SLM parts at temperatures higher than the solvus temperature of IN718's various phases ($\delta, \gamma', \gamma''$, and Laves) leads to grain growth [8]. This suggests that further refining the anneal time and temperature can potentially mitigate the anisotropy of SLM parts.

As previously stated, the material properties of SLM parts are dependent on their build orientation. While the tensile properties of SLM IN718 printed under various conditions have been well researched [3,9–11], there are limited studies regarding its fatigue life. Konečná studied the high-cycle fatigue behavior of as-built SLM IN718. He found that the SLM material is less resistant to crack growth at low K_a values but has comparable crack growth resistance at K_a values above 10 MPa $m^{1/2}$ [12]. Witkin studied the high-cycle fatigue life of a notched SLM IN718 specimen. He found that machined parts had similar fatigue behavior as traditionally manufactured IN718, while non-machined parts failed much sooner [13]. These results were also observed by Kelley [14]. Since SLM can create intricate parts with geometries that are difficult to post-process using traditional methods, a different method must be developed to improve the fatigue life of these parts. In addition to SLM, the fatigue life of IN718 parts created by electron beam melting [15] and direct laser deposition [16] have also been studied. However, none of these studies have specifically attempted to modify the microstructure to mitigate its anisotropy. The authors believe that this is the first study that focuses on improving the fatigue life of SLM IN718 by manipulating its microstructure.

This study presents fatigue life data for SLM IN718 parts printed in three different orientations (0°, 45°, and 90°). Parts built in each orientation were prepared using three different heat treatment methods (none, AMS-5662 treated, modified). The number of cycles to failure at different stress values for each test case were measured in order to produce S-N curves. The surface roughness and fracture surfaces were also analyzed to account for variations in the fatigue life. This research serves as preliminary evidence that the anisotropy inherent to SLM can be reduced by modifying the applied heat treatment.

Table 2
Summary of the laser parameters. The contours surround the inner and outer parts of the skin to create higher uniformity in the part.

Section	Laser power (W)	Spot size (μm)	Speed (mm s^{-1})
Core	370	180	700
Skin	180	130	800
Contour	120	50	280

2. Materials and methodology

2.1. Test specimens

Specimens were printed with a Concept Laser M2 cusing 3D metal printer using IN718 powder purchased from the Powder Alloy Corporation (Loveland, Ohio, USA). The powder had an average diameter of 40 μm, and its chemical composition is presented in Table 1. The specimens were printed using the island scan strategy and the skin-core method. The inner core of the part was printed with a higher power and spot size than the skin. This reduced the print time while retaining the mechanical properties of a traditionally manufactured part. The skin was approximately 2 mm thick. The associated laser parameters are presented in Table 2. The islands were 5 mm × 5 mm, and they were printed stochastically. The height of each print layer was 40 μm.

Rectangular tension test specimens were printed using ASTM E8 M [17] as a baseline and modified accordingly to prevent the mechanical test system from overloading at the set frequency. A 4 mm offset was implemented in the specimen design. The offset was included to decrease thermal stresses and increase the amount

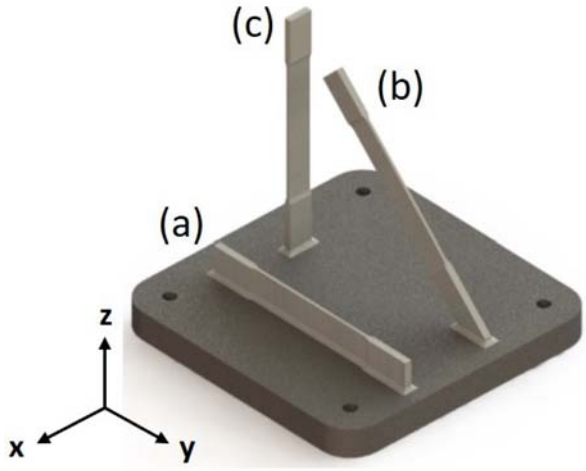

Fig. 1. Representative specimens printed using three different orientations: 0° (a), 45° (b), and 90° (c). The specimen design is based on ASTM E8M. The XY plane is transverse to the build direction, while the XZ and YZ planes are parallel to the build direction.

Table 3
Summary of the different specimen types. The modified specimens were annealed for four hours at 1160 ° C.

Specimen ID	Print orientation	Heat treatment	Quantity prepared
ASH	0°	None	4
ASD	45°	None	8
ASV	90°	None	7
AHH	0°	AMS 5662	4
AHD	45°	AMS 5662	5
AHV	90°	AMS 5662	5
AHMH	0°	Modified	7
AHMD	45°	Modified	5
AHMV	90°	Modified	4

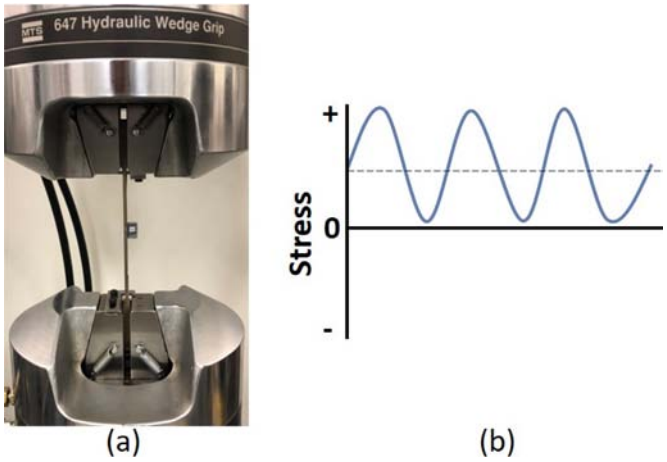

Fig. 2. Mechanical testing machine with a fatigue sample (a) that is tested in a tension-tension loading profile (b). The maximum applied load ranged between 15% and 80% of the UTS.

of thermal conduction into the build plate. The specimens were removed from the build plate using wire electrical discharge machining. The nominal dimensions of the specimens' gauge length and grips were 112 mm × 21 mm × 2.5 mm and 38 mm × 21 mm × 6 mm, respectively. Three separate specimen sets were printed: 0° (printed along the length of the specimen), 45°, and 90° (printed along the cross-sectional area of the specimen). The different print orientations are presented in Fig. 1. Four specimens were printed for the monotonic tensile tests, while four specimens were printed for each set of fatigue specimens. In some cases, additional specimens were printed to better characterize the fatigue life at low stress amplitudes. This resulted in 49 total specimens studied. A summary of the different specimen types is presented in Table 3. Four wrought IN718 specimens were also machined to these specifications to serve as a baseline of comparison for the fatigue life.

2.2. Heat treatment

Two separate heat treatments were performed for this research at Winston Heat Treating (Dayton, Ohio, USA). One set of SLM specimens

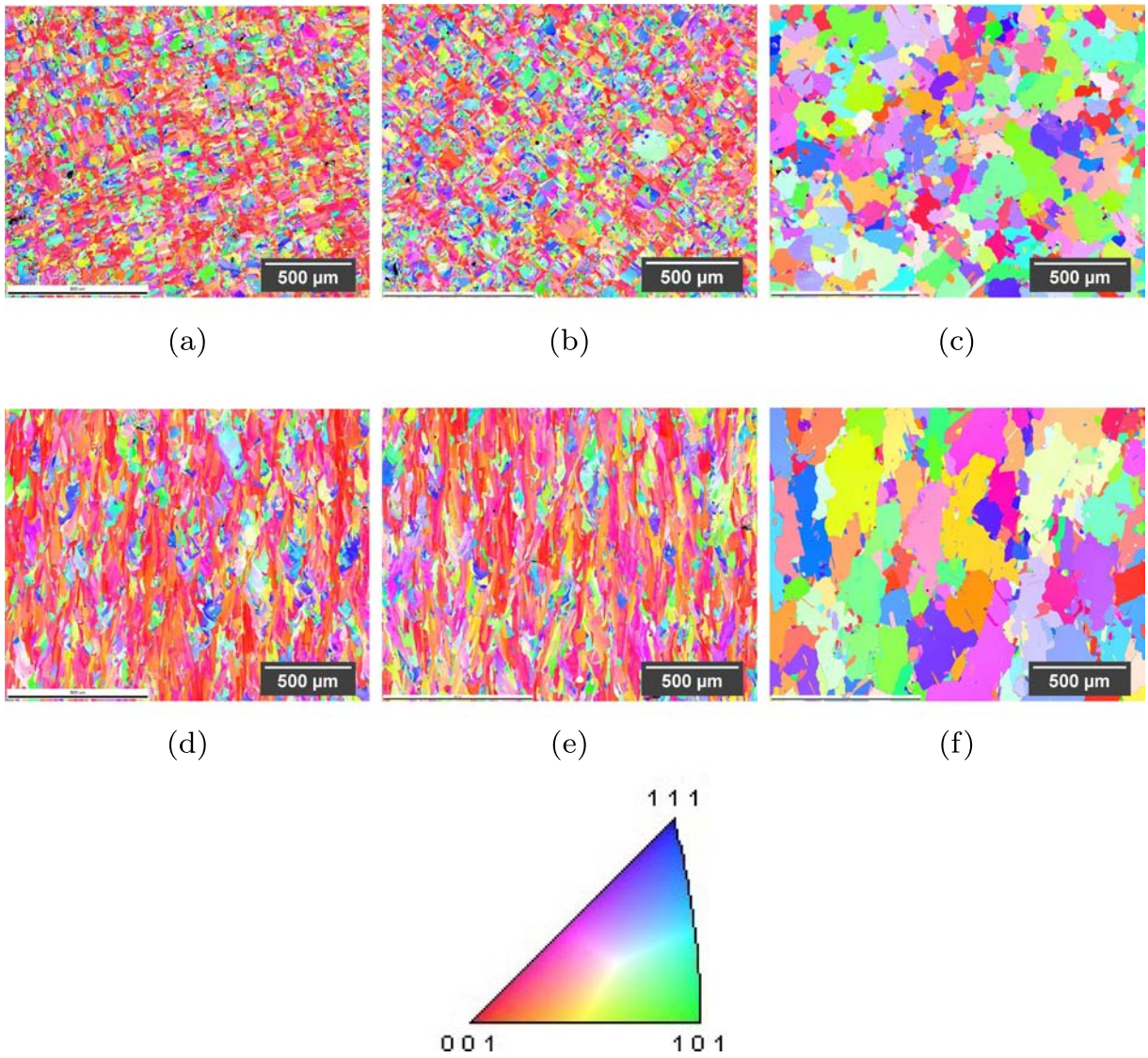

Fig. 3. Grain structure of the as-built (a,d), ASM-5662 treated (b,e) and modified heat treated (c,f) IN718 specimens. The areas presented in (a–c) are transverse to the print direction, while the areas presented in (d-f) are parallel to the print direction. The modified heat treatment increased the grain size by a factor of 2.5.

Table 4
Average grain size, grain orientation spread, and twin fraction for the three test cases. The ASM standard heat treatment does not affect these parameters, while the modified heat treatment increases them.

	Transverse to build direction			Parallel to build direction		
Specimen	Grain diameter (μm)	Recrystallization (%)	Twin fraction	Grain diameter (μm)	Recrystallization (%)	Twin fraction
As-built	9.75	29.1	0.016	12.2	19.1	0.029
ASM heat treatment	9.91	37.5	0.008	13.8	17.5	0.027
Modified heat treatment	26.03	94.3	0.215	31.57	96.6	0.262

and the wrought specimens were annealed in a vacuum furnace as specified in AMS 5662 for one hour at 1010 °C. The second set of SLM specimens was first annealed for four hours at a temperature of 1160 °C. The modified treatment's temperature is in line with the temperatures prescribed for hot isostatic pressed (HIP) IN718 found in Section 13 of ASTM F3055 [18]. Annealing IN718 at 1160 °C allows its grains to recrystallize and grow. The differences in the resulting microstructures will be further discussed in the Results section. All anneals were followed by a rapid nitrogen gas quench and subjected to a double-aging treatment as described in AMS 5663 [19]. They were aged in a vacuum furnace at 718 °C for eight hours, furnace cooled over two hours to 621 °C, held at 621 °C for an additional eight hours, and finally cooled to room temperature with air. The specimens were not HIPed or further machined after the heat treatments were applied.

2.3. Mechanical testing

Both monotonic tensile tests and fatigue tests were conducted in an MTS 810 Servo Hydraulic Machine equipped with an MTS 647 Hydraulic Wedge Grip (MTS Systems Corporation, Eden Prairie, Minnesota, USA). The grip system loaded with a specimen is presented in Fig. 2a. The system contained a load cell with a maximum capacity of 100 kN. An extensometer was attached to each of the specimens' gauge sections to measure the difference in the strain. Tensile tests were performed in force control mode at a stress rate of approximately 5 MPa s^{-1}. The fatigue tests performed were tension-tension (see Fig. 2b). They were performed in force control mode using a frequency of 10 Hz and a stress ratio, R, of 0.1. Each specimen set was tested using max stresses ranging from 15% to 80% of the ultimate tensile strength (UTS) of the as-built specimens. They were tested until failure had occurred or two weeks had elapsed. Force and displacement data were collected throughout the experiment in order to calculate the specimens' mechanical properties.

2.4. Microscopic analysis

Samples from each specimen set were prepared for electron backscatter diffraction (EBSD) analysis. The samples were mounted in a conductive phenolic resin, polished down to 1 μm using a Buehler EcoMet 300 (Illinois Tool Works, Lake Bluff, IL, USA), and further polished overnight using 0.05 μm SiO_2 solution in a Buehler VibroMet (Illinois Tool Works, Lake Bluff, IL, USA). EBSD analysis was performed with an EDAX TEAM Pegasus system (Ametek Materials Analysis Division, Mahwah, NJ, USA) in a TESCAN MAIA3 scanning electron microscope (SEM) (TESCAN, Brno, Czech Republic). The accelerating voltage of the source beam was 20 kV and the beam intensity was 20. Surface areas parallel and transverse to the build direction were analyzed in order to develop a complete picture of the specimens' grain structure. A description of both planes is presented in Fig. 1 . The chemical composition of the scanned areas was collected concurrently with the EBSD data using an energy-dispersive X-ray spectroscopy (EDS) detector (Ametek Materials Analysis Division, Mahwah, NJ, USA). Grain analysis was performed using EDAX's OIM™ Analysis software (Ametek Materials Analysis Division, Mahwah, NJ, USA).

After fatigue testing had concluded, the failure region was sectioned from the specimens for microscopic analysis. Surface roughness analysis was performed using a ZEISS LSM 700 laser scanning confocal microscope (Carl Zeiss AG, Oberkochen, Germany). The area near the failure region was analyzed to determine the specimens' average surface roughness values. A 555-nm wavelength focused laser beam was used to scan the surface, which generated a surface roughness profile based on the reflected intensity of the laser. The arithmetical mean height of the surface (S_a) was determined using this profile. Images taken at the failure region were acquired using a Tescan MAIA3 field emission SEM. The source beam had an accelerating voltage of 15 kV and a spot size of 8.1 nm.

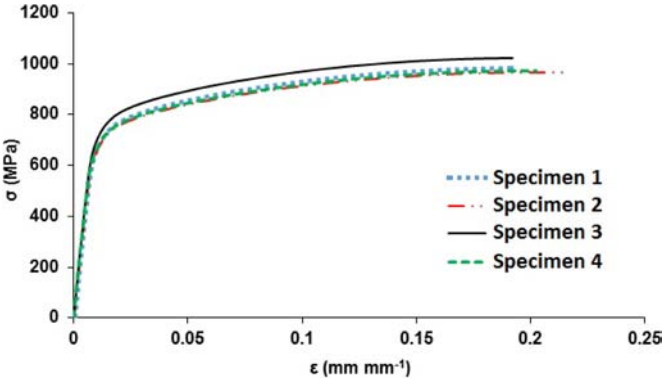

Fig. 4. Stress-strain data for as-built AM specimens. The overlap seen in the curves indicates that the printing process was very consistent.

3. Results and discussion

3.1. Grain analysis

The grain properties of the different specimen sets were analyzed using EBSD. The EBSD maps collected from the 0° specimens are presented in Fig. 3, while grain analysis data is presented in Table 4. The grain maps and data for the 45° and 90° specimens were similar to those presented in Fig. 3 and will not be presented. The grains of the as-built (Fig. 3a and d) and ASM-5662 treated (Fig. 3b and e) specimens are very similar in shape and size for both the parallel and transverse planes, which is expected based on previous research [5–7]. Both maps display small, equiaxed grains in the transverse plane (Fig. 3a and b) and long, columnar grains in the parallel plane (Fig. 3d and e). The grain maps of the modified heat treated specimens (Fig. 3c and f) resemble the grain maps typically reported for wrought specimens. The grains of the modified heat treatment were larger than both the as-built and ASM-5662 treated specimens'

Table 5
Mechanical properties of the as-built 0° specimens. These results were used to calculate a baseline for the alternating stresses studied.

UTS (MPa)	Yield strength (MPa)	Elastic modulus (GPa)	Elongation (mm mm^{-1})
986 ± 26	602 ± 18	89 ± 2	0.2 ± 0.01

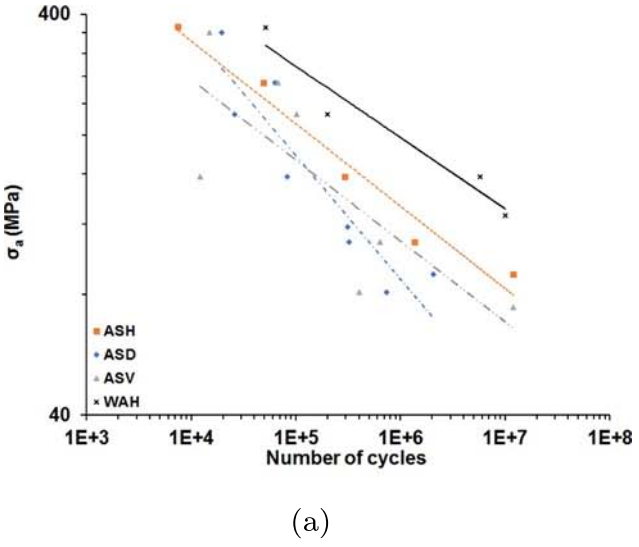

(a)

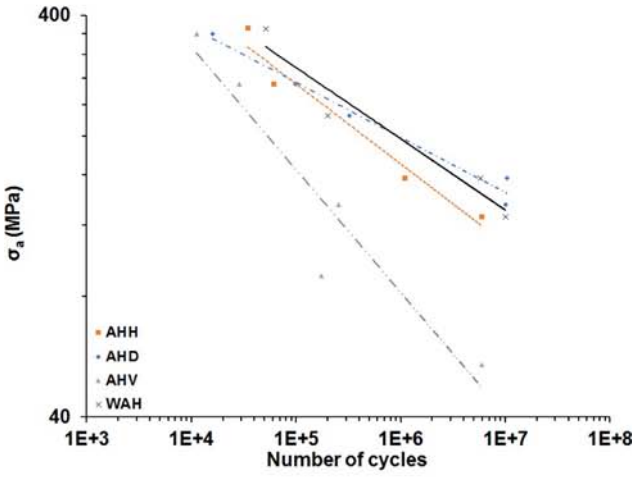

(b)

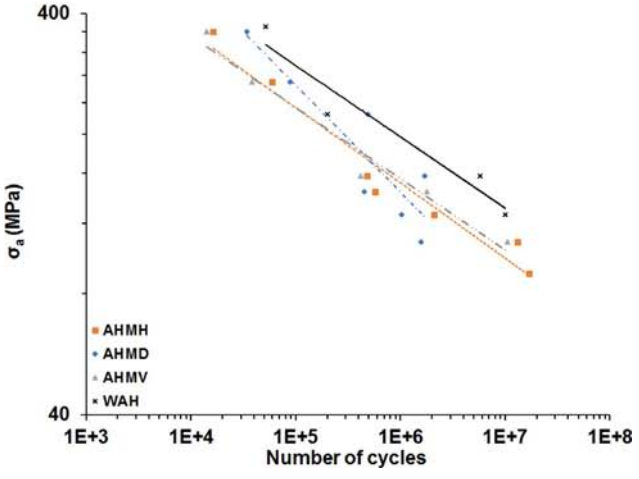

(c)

Fig. 5. S-N curves for the as-built (a), ASM-5662 treated (b), and modified heat treated (c) specimens. Both axes are scaled logarithmically and do not begin at the origin. The S-N curve for wrought heat treated IN718 specimens (WAH) is also included as a baseline for comparison.

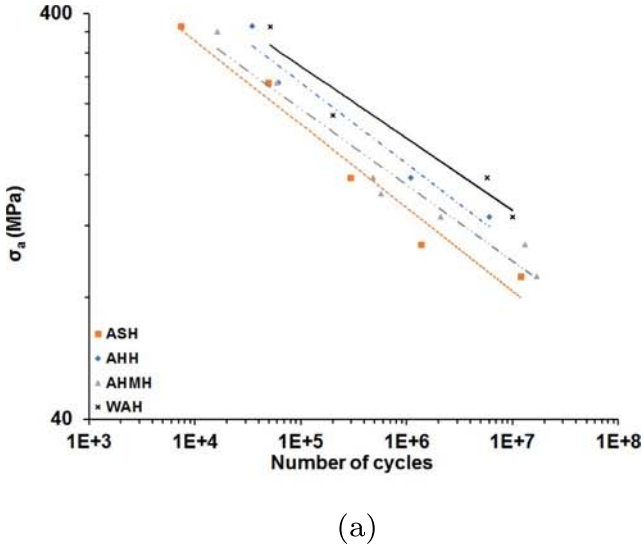

(a)

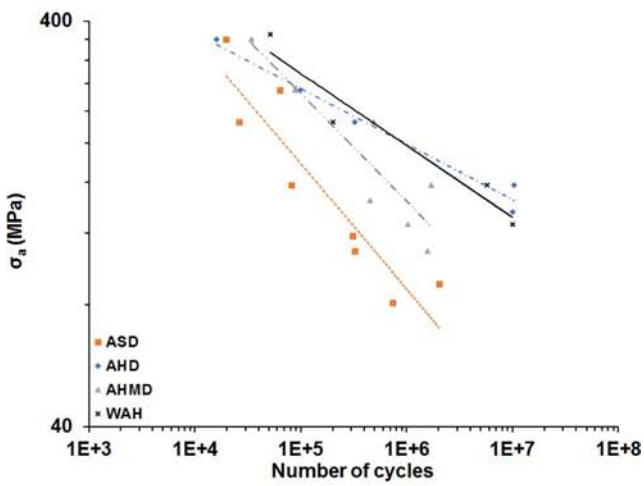

(b)

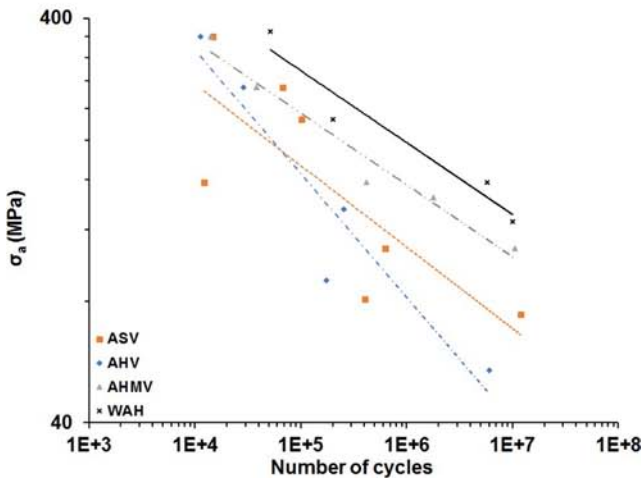

(c)

Fig. 6. S-N curves for the 0° (a), 45° (b), and 90° (c) specimens. Both axes are scaled logarithmically and do not begin at the origin. The S-N curve for wrought heat treated IN718 specimens (WAH) is also included as a baseline for comparison.

Table 6
Parameters for the S-N curve equation. The relationship was modeled using a power law. Wrought heat treated specimens (WAH) are also included for comparison.

Specimen	A	B
ASH	2283.6	−0.206
ASD	5035.1	−0.293
ASV	1761.1	−0.201
AHH	2686.3	−0.199
AHD	1324.7	−0.137
AHV	5577.6	−0.306
AHMH	2179.4	−0.194
AHMD	5692.4	−0.266
AHMV	1812.2	−0.178
WAH	2301.6	−0.178

grains by a factor of 2.5. This was true for both the transverse and parallel planes.

The grain orientation spread (GOS) was used to calculate the degree of recrystallization presented in Table 4. The GOS characterizes the amount of misorientation in a grain and is used to quantify the amount of recrystallization in metals [20]. A misorientation angle of 1.2° was selected as the threshold for recrystallization. This threshold was selected based on research performed by Cao [21]. The percentage of grains in the EBSD map with a GOS <1.2° for the as-built specimens was 29.1% and 19.1% for the transverse and parallel planes, respectively. The ASM-5662 treated specimens had similar degrees of recrystallization (37.5% and 17.5%), while the modified heat treated specimens' degrees of recrystallization were much higher (94.3% and 96.6%).

The twin fraction was also measured for each test case. None of the planes of the as-built or ASM-5662 treated specimens had a twinning fraction that exceeded 0.03 (see Table 4). However, the amount of twinned grains in the modified heat treated specimens was 0.215 for the transverse plane and 0.262 for the parallel plane. These values are comparable to the twin fractions for wrought specimens with similar grain sizes studied by Jin [22]. The increased grain sizes, degrees of recrystallization, and twin fractions of the modified heat treated specimens confirm that the modified heat treatment significantly changed the microstructure of SLM IN718.

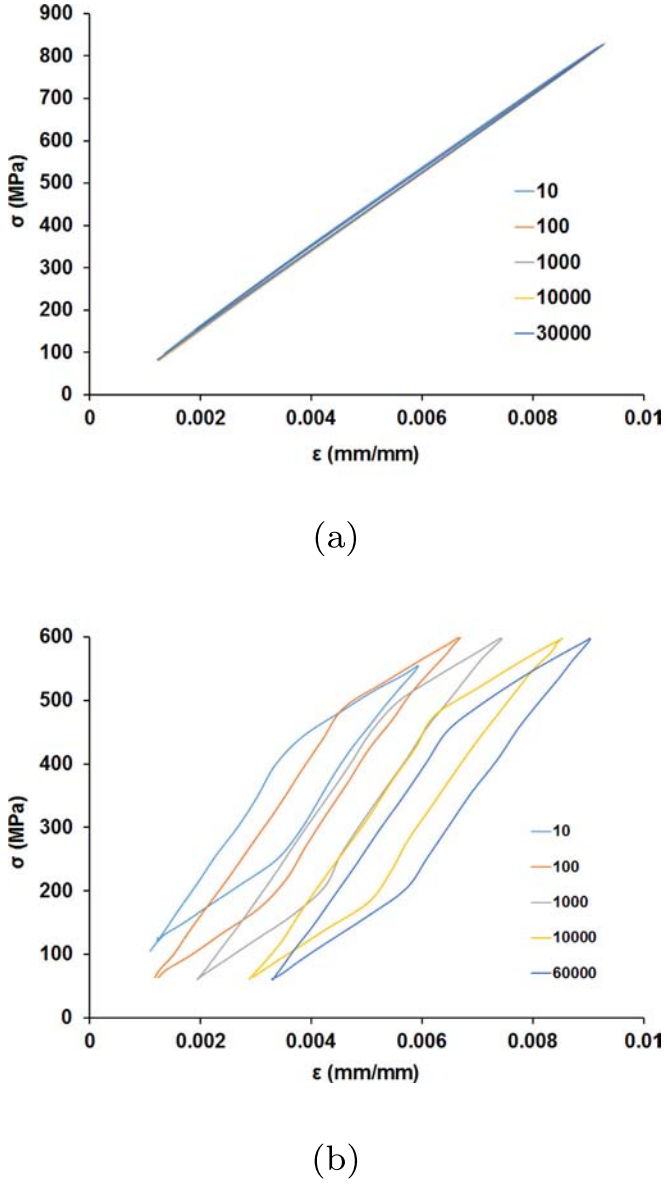

Fig. 7. Representative specimens exhibiting fully elastic deformation (a) and elastic-plastic deformation (b).

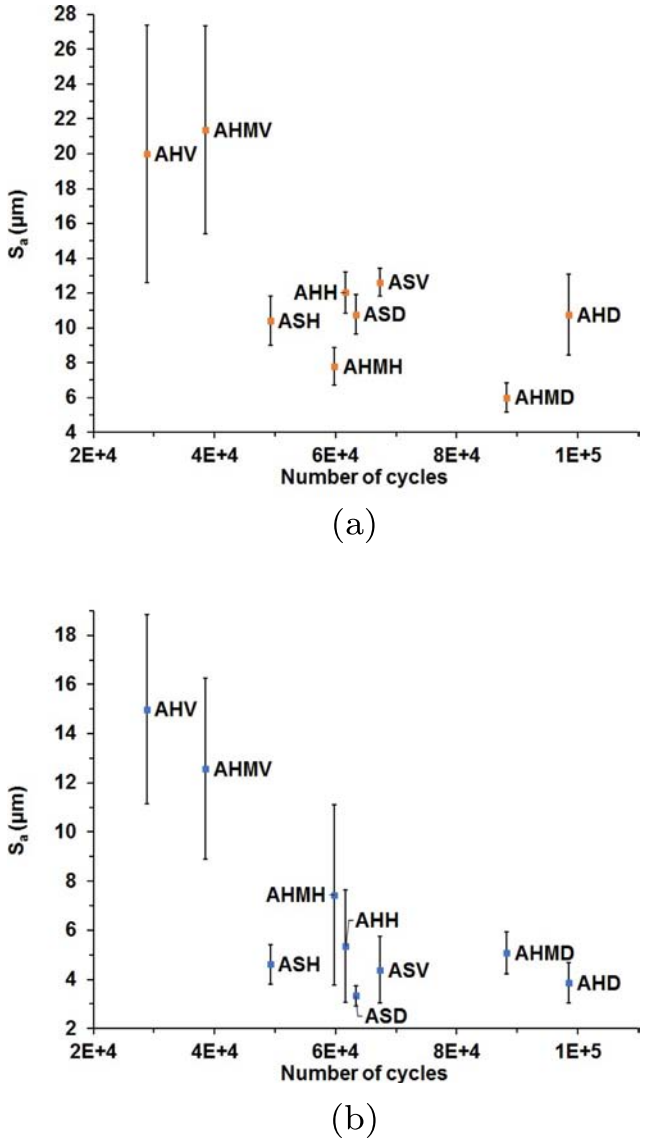

Fig. 8. S_a values for the fatigue specimens ($\sigma_a = 270$ MPa) measured across a 1.4 mm^2 (a) and 0.1 mm^2 (b) area. Higher S_a values show a correlation to lower fatigue lives.

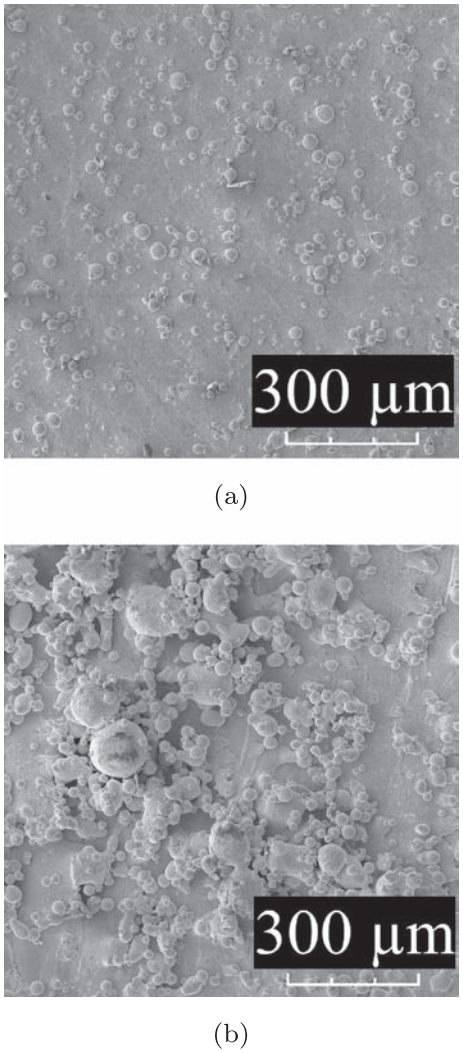

Fig. 9. Micrographs of fatigue specimen surfaces. The average S_a value of (a) is 6.00 μm, while the average S_a value of (b) is 21.37 μm. The large particles found in (b) act as potential stress concentration areas that reduce the specimens' fatigue life.

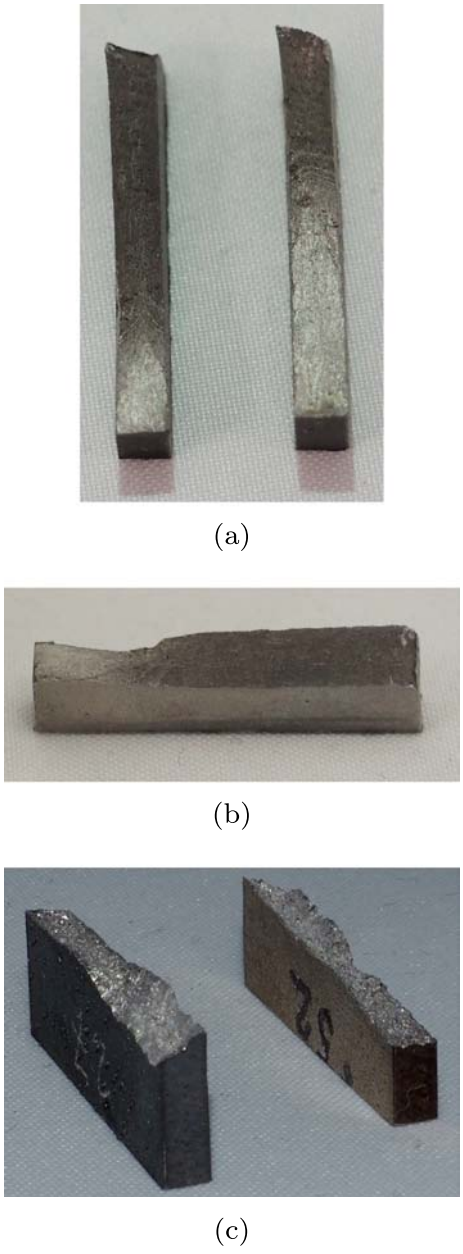

Fig. 10. Representative failed specimens after undergoing high cyclic loading (left) and low cyclic loading (right) (a). Note that the length of the crack surface (shiny areas) is inversely proportional to the applied stress. Side view of the specimen subjected to high cyclic loading (b). The dark area has a 45° slope, which indicates that shear deformation occurred. Comparison of the fatigue surface of the 0° (left) and 90° (right) specimens (c). The area where shear deformation occurred is more pronounced in the 0° and 45° specimens.

Chemical analysis was also performed with EDS for the six test cases. The chemical composition of the as-built and ASM-5662 treated specimens was evenly distributed across the measured area. In contrast, the modified heat treated specimens had regions that were niobium rich. The Nb-rich regions are believed to be carbides due to their shape and size. None of the other phases found in wrought IN718 were detectable using EDS.

3.2. Monotonic tensile and fatigue tests

Tensile data were measured for the as-built 0° specimens. The stress-strain curves calculated from this data is presented in Fig. 4. The curves show that there was a high degree of consistency between samples. A summary of the mechanical properties is presented in Table 5. The strength values closely match previous research [23]. A baseline value of 1 GPa was selected to calculate the alternating stresses (σ_a) studied.

Fig. 5presents S-N curves for as-built, ASM-5662 treated, and modified heat treated specimens. This data was rearranged based on print orientation in Fig. 6. Both axes are scaled logarithmically. Fatigue data for wrought specimens heat treated as outlined in ASM 5662 and ASM 5663 are also presented in each graph as a baseline for comparison. The S-N curves presented in Figs. 5 and 6 were modeled using a power function in the form

$$\sigma_a = AN^B, \tag{1}$$

where σ_a is the alternating stress, N is the number of cycles, and A and B are constants. The values of A and B for each test case are presented in Table 6.

In almost all cases, the fatigue life of the SLM specimens did not surpass the fatigue life of wrought IN718. The as-built specimens performed the worst out of the three sets, and the predicted wrought specimens' fatigue life was at least one order of magnitude greater

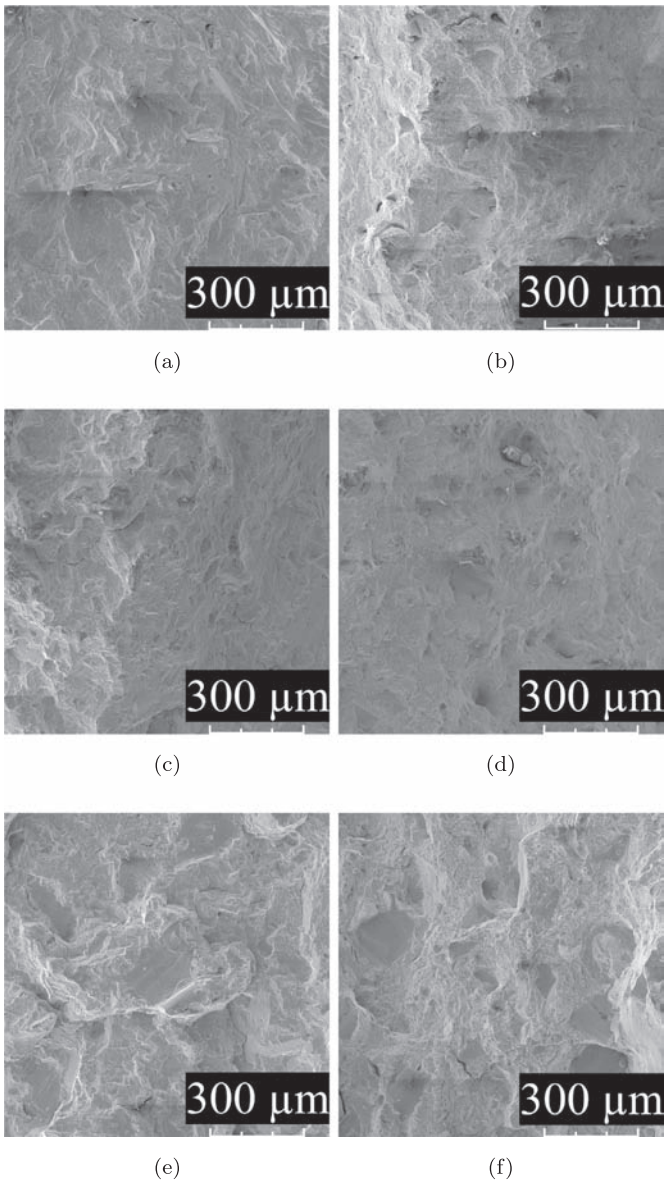

Fig. 11. Failure regions of the 0° (a,b), 45° (c,d) and 90° (e,f) specimens. Crack propagation occurred in areas (a,c,e), while failure caused by overloading occurred in areas (b,d,f). Smooth areas where layer adhesion did not occur are the most prevalent in the 90° specimens.

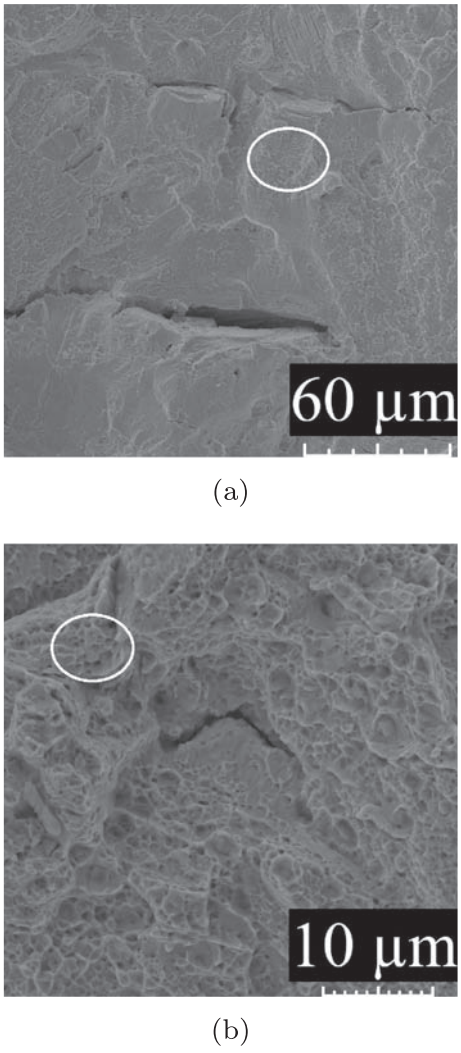

Fig. 12. High magnification fractographs of the crack propagation region (a) and stress overloading region (b). The area in (a) contains regions with fatigue striations, while (b) contains characteristic dimples associated with elastic failure.

than all of the predicted as-built specimens at any given σ_a (see Fig. 5a). Both heat treatments improved the fatigue life of the SLM specimens. The 0° and 45° AMS-5662 treated specimens had fatigue lives that were better than the corresponding modified heat treated specimens, while the 90° AMS-5662 specimens' fatigue life was much lower than the fatigue life of the modified heat treated specimens. There was also a great degree of variation within the observed fatigue limits. Although most specimens survived when σ_a was less than 90 MPa, the as-built and modified heat treated 45° specimens did not. Conversely, the AMS-5662 treated 45° specimens' fatigue limit exceeded all other specimens. Additional research should be performed to determine if the observed range of the fatigue limit resulted from the build orientation, the applied heat treatment, or other outside factors.

As previously noted, the modified heat treatment was introduced in order to mitigate the anisotropic behavior of SLM IN718 specimens caused by the build orientation. While the fatigue life of the modified heat treated specimens did not surpass the fatigue life of the AMS-5662 treated specimens, it did reduce the anisotropy caused by the build orientation. This is evident in the 0° and 90° specimens. Both the individual data points as well as the predictive S-N curves nearly overlap in Fig. 5c. Further modifications to the applied heat treatment would likely reduce the anisotropy present in the 45° specimens.

The stress-strain data was plotted in order to generate hysteresis loops for the test samples. Representative curves are presented in Fig. 7. All of the 45° and 90° specimens exhibited the plastic and elastic loading and unloading shown in Fig. 7b, while the 0° specimens' behavior varied based on the heat treatment. All of the as-built 0° specimens and the AMS-5662 treated 0° specimens with loads ≥ 35% of the UTS exhibited an almost entirely elastic response during testing (Fig. 7a), while the response of the modified heat treated specimens was similar to the 45° and 90° specimens. This further indicates that the modified heat treatment creates parts with more isotropic microstructures and mechanical properties.

3.3. Surface roughness

The surface properties of a material directly affect its fatigue life. Common loading failures initially occur at a material's surface, and

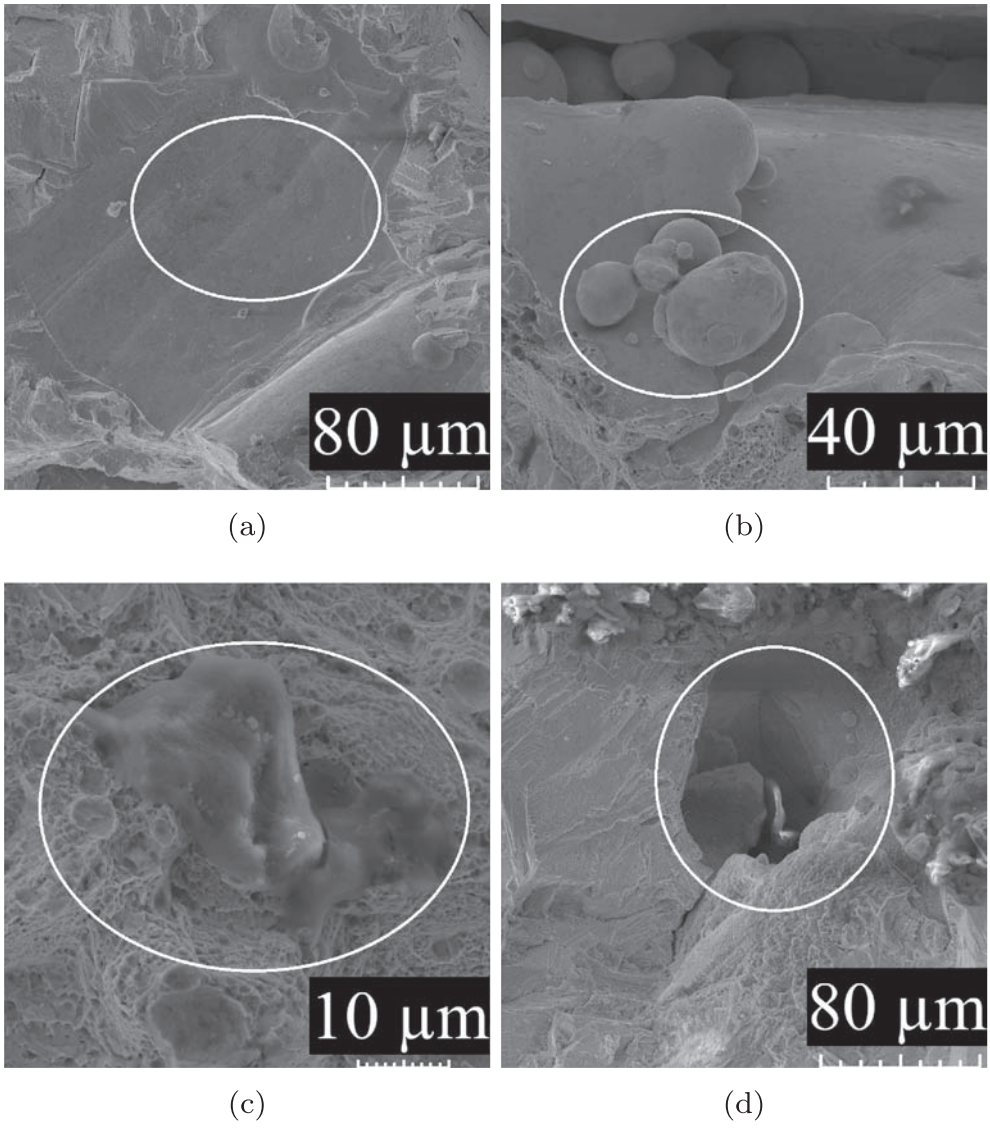

Fig. 13. Example defects including unadhered layers (a), partially sintered and unsintered particles (b), carbides (c), and pores (d). These defects can serve as locations where cracks can form internally, which would ultimately reduce a specimen's fatigue life.

higher strength materials such as IN718 are disproportionately sensitive to surface defects [24]. The surface topography of an SLM part can be affected by factors such as particle sizing effects, melt pool dynamics, and location on the build plate. Excessive surface roughness can be removed by post-processing but, as previously stated, this can be difficult to perform if a part has intricate features. The modified heat treatment was introduced to attempt to eliminate the need for further post-processing. In order to determine the dominating factor that will predict a part's fatigue life, surface roughness must be studied in addition to the applied heat treatment.

The surface roughness versus the number of cycles to failure is presented in Fig. 8. The specimens in Fig. 8 were all tested at an alternating stress of 270 MPa. Two separate surface areas (0.1 mm^2 and 1.4 mm^2) were measured to compare the overall surface roughness values versus the localized surface roughness values. Each sample was measured at five different areas near the failure region to generate the error bars seen in Fig. 8. Examples of specimens with high and low S_a are presented in Fig. 9. The specimens with the highest S_a values had the shortest fatigue lives. However, once a certain roughness threshold is surpassed, the build orientation appears to be the main factor that determines the fatigue life. This trend was also noted in other specimen sets. Further research is required to define the transition region where build orientation surpasses S_a as the dominating factor for predicting fatigue life.

3.4. Fracture surface

The fracture surfaces of the failed specimens were analyzed and compared. All of the specimens exhibited distinct failure regions. The regions where the crack propagation occurred are shiny, while failure caused by overloading occurred in the matte areas. The shininess of the crack propagation region is caused by the high reflectivity of flat cleavage facets generated while cyclic loading occurred. Representative optical images of these regions are presented in Fig. 10a. Crack initiation typically occurred in the corner of the specimens. The matte regions were angled at 45°, which indicates that overloading caused shear deformation. An example of the observed shear deformation is presented in Fig. 10b. The shear deformation was less pronounced in the 90° specimens (see Fig. 10c), for reasons that will be explained in a later paragraph.

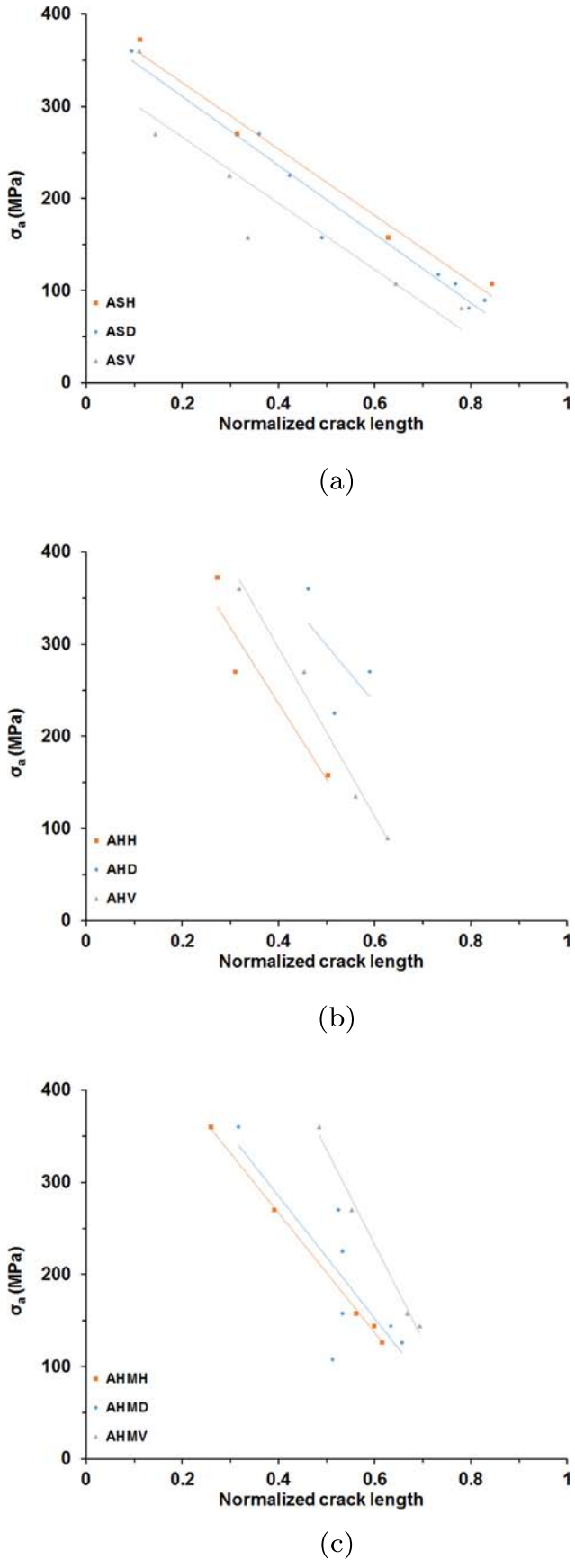

Fig. 14. Total crack length versus the stress amplitude for the as-built (a), ASM-5662 treated (b), and modified heat treated (c) specimens. The crack length has been normalized to their respective specimens' widths.

Scanning electron fractographs of both the crack propagation region and overloaded region of the different specimens are presented in Fig. 11. Higher magnification fractographs of the crack propagation and overloading regions are presented in Fig. 12. The area where the crack propagated has fatigue striations (Fig. 12a), while the surface of the area where overloading occurred has dimples (Fig. 12b). This confirms that shear deformation occurred at the overloaded region. While both transgranular and intergranular crack formation occurs throughout the specimen, the majority of the failure is elastic-plastic and intergranular. There were no observable differences in the scanning electron fractographs of the as-built and heat treated specimens.

There were various defects detected on the fracture surfaces, and these defects are presented in Fig. 13. One such defect was the presence of unadhered areas. These areas are created when the laser cannot fully penetrate both the powder layer and the substrate layer. The resulting substrate layer is smooth (see Fig. 13a). The unadhered areas were most prevalent in the 90° specimens (see Fig. 11e and f). This is the likely cause for the less pronounced shear deformations found in Fig. 10c, since each unadhered region could act as an area where cracks can initiate and propagate. Their size and shape were directly affected by the print orientation. The unadhered areas of the 90° specimens were large and circular, while they were smaller and elliptical in the 0° specimens. Other defects that were observed include unsintered particles (Fig. 13b), carbides (Fig. 13c), and pores (Fig. 13d). All of these defects could ultimately reduce the fatigue life of the specimens as compared to the wrought specimens, since they could serve as sites for damage nucleation [25]. Neither heat treatment appears to have affected the presence or number of defects in the specimens.

Fig. 14 shows the length of the crack surface versus σ_a for the as-built (14a), ASM-5662 treated (14b), and modified heat treated (14c) specimens. The crack lengths were normalized to allow for direct one-to-one comparison. The crack length for all of the specimens increased as σ_a decreased. The crack growth over the σ_a range was more gradual for the as-built specimens than the AMS-5662 or modified heat treated specimens. At high fatigue loads, the cracks of the heat treated specimens grew to a greater length than the cracks of the as-built specimens. This is due to the improved strength of the material caused by heat treatments. However, at low fatigue loads, the as-built specimens have higher crack lengths at failure. This is possibly due to a reduction in ductility of the specimens caused by the heat treatment.

4. Conclusions

The fatigue life of as-printed, ASM-5662 treated, and modified heat treated SLM IN718 specimens printed at different orientations was studied. The modified heat treatment was developed to mitigate the specimens' anisotropic mechanical properties by modifying their microstructure. EBSD revealed that the modified heat treatment caused the specimens' grains to increase by a factor of 2.5 and become highly crystallized while eliminating the columnar grain structure typically found in as-built SLM materials. Both heat treatments improved the fatigue lives of the specimens, and the fatigue lives of the modified heat treated 0° and 90° specimens were nearly identical. Laser scanning microscopy revealed that there is a roughness threshold that determines if the surface roughness or the build orientation accurately predicts the fatigue life. Failure analysis revealed that the print orientation has a greater affect on crack development and growth than the heat treatment. This research shows preliminary evidence that the anisotropic mechanical properties of SLM printed specimens, including their fatigue behavior, can be mitigated by modifying the standard wrought alloy heat treatment.

CRediT authorship contribution statement

Volodymyr P. Sabelkin: Conceptualization, Methodology, Validation, Formal analysis, Investigation, Writing - original draft. **Gregory R. Cobb:** Formal analysis, Writing - original draft, Writing - review & editing, Visualization. **Travis E. Shelton:** Investigation, Visualization. **Megan N. Hartsfield:** Investigation. **David J. Newell:** Conceptualization, Methodology. **Ryan P. OHara:** Supervision. **Ryan A. Kemnitz:** Supervision.

Acknowledgments

The authors would like to thank the Oak Ridge Institute for Science and Education (ORISE) for the research associateships granted to Dr. Volodymyr P. Sabelkin, Mr. Gregory R. Cobb, and Ms. Megan N. Hartsfield.

Data Availability

The datasets generated and/or analyzed during the current study are available from the corresponding author on reasonable request.

References

[1] C.Y. Yap, C.K. Chua, Z.L. Dong, Z.H. Liu, D.Q. Zhang, L.E. Loh, S.L. Sing, Review of selective laser melting: materials and applications, Appl. Phys. Rev. 2 (4) (2015) 041101. https://doi.org/10.1063/1.4935926.

[2] T.M. Mower, M.J. Long, Mechanical behavior of additive manufactured, powder-bed laser-fused materials, Mater. Sci. Eng. A 651 (2016) 198–213. http://www.sciencedirect.com/science/article/pii/S092150931530530X. https://doi.org/10.1016/j.msea.2015.10.068.

[3] K. Amato, S. Gaytan, L. Murr, E. Martinez, P. Shindo, J. Hernandez, S. Collins, F. Medina, Microstructures and mechanical behavior of Inconel 718 fabricated by selective laser melting, Acta Mater. 60 (5) (2012) 2229–2239. https://linkinghub.elsevier.com/retrieve/pii/S1359645411008949. https://doi.org/10.1016/j.actamat.2011.12.032.

[4] SAE International, Nickel Alloy, Corrosion and Heat-Resistant, Bars, Forgings, and Rings 52.5Ni - 19Cr - 3.0Mo - 5.1Cb (Nb) - 0.90Ti - 0.50Al - 18Fe Consumable Electrode or Vacuum Induction Melted 1775 F (968 C) Solution Heat Treated, Precipitation-Hardenable AMS5662N, 2016, https://www.sae.org/standards/content/ams5662n/.

[5] M. Pröbstle, S. Neumeier, J. Hopfenmüller, L. Freund, T. Niendorf, D. Schwarze, M. Göken, Superior creep strength of a nickel-based superalloy produced by selective laser melting, Mater. Sci. Eng. A 674 (2016) 299–307. https://linkinghub.elsevier.com/retrieve/pii/S092150931630822X. https://doi.org/10.1016/j.msea.2016.07.061.

[6] J. Strößner, M. Terock, U. Glatzel, Mechanical and microstructural investigation of nickel-based superalloy IN718 manufactured by Selective Laser Melting (SLM), Adv. Eng. Mater. 17 (8) (2015) 1099–1105. http://doi.wiley.com/10.1002/adem.201500158. https://doi.org/10.1002/adem.201500158.

[7] J. Schneider, B. Lund, M. Fullen, Effect of heat treatment variations on the mechanical properties of Inconel 718 Selective Laser Melted specimens, Additive Manufacturing 21 (2018) 248–254. https://linkinghub.elsevier.com/retrieve/pii/S2214860417306218. https://doi.org/10.1016/j.addma.2018.03.005.

[8] S. Raghavan, B. Zhang, P. Wang, C.-N. Sun, M.L.S. Nai, T. Li, J. Wei, Effect of different heat treatments on the microstructure and mechanical properties in selective laser melted INCONEL 718 alloy, Mater. Manuf. Process. 32 (14) (2017) 1588–1595. https://www.tandfonline.com/doi/full/10.1080/10426914.2016.1257805. https://doi.org/10.1080/10426914.2016.1257805.

[9] D. Ivanov, A. Travyanov, P. Petrovskiy, V. Cheverikin, E. Alekseeva, A. Khvan, I. Logachev, Evolution of structure and properties of the nickel-based alloy EP718 after the SLM growth and after different types of heat and mechanical treatment, Addit. Manuf. 18 (2017) 269–275. http://www.sciencedirect.com/science/article/pii/S2214860417301513. https://doi.org/10.1016/j.addma.2017.10.015.

[10] T. Trosch, J. Strößner, R. Völkl, U. Glatzel, Microstructure and mechanical properties of Selective Laser Melted Inconel 718 compared to forging and casting, Mater. Lett. 164 (2016) 428–431. http://www.sciencedirect.com/science/article/pii/S0167577X15307850. https://doi.org/10.1016/j.matlet.2015.10.136.

[11] D. Zhang, W. Niu, X. Cao, Z. Liu, Effect of standard heat treatment on the microstructure and mechanical properties of Selective Laser Melting manufactured Inconel 718 superalloy, Mater. Sci. Eng. A 644 (2015) 32–40. http://www.sciencedirect.com/science/article/pii/S0921509315300745. https://doi.org/10.1016/j.msea.2015.06.021.

[12] R. Konečná, L. Kunz, G. Nicoletto, A. Bača, Fatigue crack growth behavior of Inconel 718 produced by selective laser melting, Int. J. Fatigue 10 (2016) 31–40. https://doi.org/10.3221/IGF-ESIS.36.04.

[13] D. Witkin, D. Patel, G. Bean, Notched fatigue testing of Inconel 718 prepared by Selective Laser Melting, Fatigue Fract. Eng. Mater. Struct. 42 (1) (2019) 166–177. https://onlinelibrary.wiley.com/doi/abs/10.1111/ffe.12880. https://doi.org/10.1111/ffe.12880.

[14] P. Kelley, A. Saigal, A. Carter, Fatigue behavior of direct metal laser sintered Inconel 718, Inter. J. Prec. Tech. 6 (3/4) (2016) 277–288. https://www.inderscienceonline.com/doi/abs/10.1504/IJPTECH.2016.080001. https://doi.org/10.1504/IJPTECH.2016.080001.

[15] M. Kirka, D. Greeley, C. Hawkins, R. Dehoff, Effect of anisotropy and texture on the low cycle fatigue behavior of Inconel 718 processed via electron beam melting, Int. J. Fatigue 105 (2017) 235–243. http://www.sciencedirect.com/science/article/pii/S014211231730350X. https://doi.org/10.1016/j.ijfatigue.2017.08.021.

[16] A.S. Johnson, S. Shao, N. Shamsaei, S.M. Thompson, L. Bian, Microstructure, fatigue behavior, and failure mechanisms of direct laser-deposited Inconel 718, JOM 69 (3) (2017) 597–603. https://doi.org/10.1007/s11837-016-2225-2.

[17] ASTM International, ASTM E8 / E8M-16a, Standard Test Methods for Tension Testing of Metallic Materials, (2016) https://doi.org/10.1520/E0008_E0008M-16A.

[18] ASTM International, ASTM F3055-14a, Standard Specification for Additive Manufacturing Nickel Alloy (UNS N07718) with Powder Bed Fusion, 2016. https://doi.org/10.1520/F3055-14A.

[19] SAE International, Nickel Alloy, Corrosion and Heat-Resistant, Bars, Forgings, and Rings 52.5Ni - 19Cr - 3.0Mo - 5.1Cb (Nb) - 0.90Ti - 0.50Al - 18Fe Consumable Electrode or Vacuum Induction Melted 1775 ° F (968 ° C) Solution and Precipitation Heat Treated AMS5663N, (2016) https://www.sae.org/standards/content/ams5663n/.

[20] S.I. Wright, M.M. Nowell, D.P. Field, A review of strain analysis using electron backscatter diffraction, Microsc. Microanal. 17 (3) (2011) 316329. https://doi.org/10.1017/S1431927611000055.

[21] Y. Cao, H. Di, J. Zhang, J. Zhang, T. Ma, R. Misra, An electron backscattered diffraction study on the dynamic recrystallization behavior of a nickel-chromium alloy (800H) during hot deformation, Mater. Sci. Eng. A 585 (2013) 71–85. http://www.sciencedirect.com/science/article/pii/S092150931300796X. https://doi.org/10.1016/j.msea.2013.07.037.

[22] Y. Jin, M. Bernacki, A. Agnoli, B. Lin, G.S. Rohrer, A.D. Rollett, N. Bozzolo, Evolution of the annealing twin density during δ – *Supersolvus* grain growth in the nickel-based superalloy Inconel™ 718, Metals 6 (1). (2016) http://www.mdpi.com/2075-4701/6/1/5. https://doi.org/10.3390/met6010005.

[23] E. Chlebus, K. Gruber, B. Kunicka, J. Kurzac, T. Kurzynowski, Effect of heat treatment on the microstructure and mechanical properties of Inconel 718 processed by selective laser melting, Mater. Sci. Eng. A 639 (2015) 647–655. http://www.sciencedirect.com/science/article/pii/S0921509315005687. https://doi.org/10.1016/j.msea.2015.05.035.

[24] W.D. Callister, D.G. Rethwisch, Materials Science and Engineering: An Introduction, 9th ed., Wiley. 2014.

[25] P.P. Milella, Fatigue and Corrosion in Metals, Springer Science & Business Media. 2012.